Effect of Ti Speciation on Catalytic Performance of TS-1 in the Hydrogen Peroxide to Propylene Oxide Reaction

The Effect of Ti Speciation on Catalytic Performance of TS-1 in the HPPO Reaction

Matteo Signorile[1], Valentina Crocellà[1], Alessandro Damin[1], Barbara Rossi[2], Carlo Lamberti[3,4], Francesca Bonino[1], and Silvia Bordiga[1]*

[1] Department of Chemistry, NIS and INSTM Reference Centre, Università di Torino, Via G. Quarello 15, I-10135 and Via P. Giuria 7, I-10125, Torino, Italy

[2] Elettra-Sincrotrone Trieste S.C.p.A. Strada Statale 14 - km 163,5 in AREA Science Park 34149 Basovizza, Trieste, Italy

[3] Department of Physics and NIS Centre, University of Turin, via Giuria 1, 10125 Torino, Italy

[4] Smart Materials Center, Southern Federal University, Zorge Street 5, 344090 Rostov-on-Don, Russia

* Corresponding author: Francesca Bonino, francesca.bonino@unito.it

Abstract

Hydrogen Peroxide to Propylene Oxide (HPPO) reaction is an attractive process exploiting Titanium Silicalite-1 (TS-1) as catalyst in combination with aqueous hydrogen peroxide as oxidizing agent. Beyond the industrial interest, TS-1 represents one of the most widely characterized catalyst due to its unique properties. However, a unified description on the

speciation of the different Ti species and their correlation to catalytic performances is missing in the literature. This work aims to exploit spectroscopic techniques (namely Diffuse Reflectance UV-VIS, Raman, FT-IR and Ti K-edge XANES) in a qualitative and quantitative way to thoroughly characterize Ti sites in a selected set of industrially relevant TS-1 samples, each one owning a peculiar Ti speciation. The outcomes of this study have been then related to the activity of each catalyst in HPPO reaction, showing its linear correlation with the content of perfect Ti sites (*i.e.* isomorphously substituting Si in the zeolitic framework). Other Ti species, such as amorphous TiO_x and bulk titania, are instead not involved in the peroxide conversion (neither in a detrimental way).

1. Introduction

Titanium Silicalite-1 (TS-1), a synthetic zeotype where titanium atoms are introduced as isomorphous substituent of the tetrahedral silicon sites in a purely siliceous MFI zeolite,[1] is an important selective catalyst in low temperature partial oxidation reactions. Being used in combination with aqueous solutions of hydrogen peroxide, TS-1 is able to catalyze selective oxidation reactions for a large variety of organic substrates with minimal byproducts production, such as the epoxidation of alkenes[2–11] and other allylic/aromatic compounds (alcohols, aldehydes, ketones).[12–20] Among these, the conversion of propylene to propylene oxide through the Hydrogen Peroxide to Propylene Oxide (HPPO) reaction[4–6,10] is one of the most investigated processes as it is an economically and ecologically superior technology since, potentially, water is the only waste product.[21] The industrial process (as independently developed by Evonik/Uhde and BASF/Dow Chemical) exploits fixed bed reactors operating in continuous flow conditions.[6]

Even if plain TS-1, as originally synthesize by its inventors, already exhibits high performances in partial oxidations, along the years many academic and industrial studies have attempted to further improve them. Excluding improvements related to the process and reaction conditions (indeed falling outside the focus of this work), two fundamental research lines mainly dealt with the increase of TS-1 performances: i) the improvement of the microporous TS-1 transport properties by inducing additional porosities and/or peculiar morphologies; and ii) the final elucidation of the catalytic role of the possible Ti species present in TS-1 to tune the syntheses in order to favor the formation of the most active ones.

The introduction of meso- and/or macro-porosities in the microporous network of a plain TS-1 ensures the enhancement of the catalytic properties, mainly due to the overall improvement of the catalyst transport properties.[22–35] Another route to achieve similar results is to shorten the diffusion path along the microporous system by decreasing the size of the TS-1 crystals.[36–38]

Concerning the study of the different Ti species, in the last decades the research topic was mostly focused on the characterization, with both experimental[8,39–48] and computational[49–57] methods, of the perfect Ti sites and on their interaction with H_2O_2 to form the active Ti-peroxo species. Nowadays, the research interest is progressively shifting toward the characterization of non-perfect Ti species.[37,43,58–62] In fact, the synthesis of a perfect TS-1 (*i.e.* where all the introduced Ti is effectively substituting the Si) is rather complex and, depending on the Ti loading and on the synthetic route, often the "non-perfect" TS-1 show different Ti species other than ones in framework positions (*i.e* tetrahedral) such as the so called "amorphous" species[58,60], supposed pentacoordinated or hexacoordinated TiO_x and antase-like clusters.[43,60] In the worst case, normally observed for high Ti loading (*e.g.* larger then ~3 wt% of TiO_2),[63] a wide fraction of titanium is transformed in a bulk oxide phase (*i.e.* titania). Amorphous pentacoordinated or

hexacoordinated TiO_x species, whose fingerprints have been recognized by means of several techniques, are still object of debate in the scientific community since their exact structures are unknown.[37,43,58–62]

What has been understood is that these particular Ti species most probably own a higher coordination with respect to the perfect tetrahedral framework Ti (*e.g.* five- or six-folded). Likely, they are no longer single Ti site (*e.g.* Ti-O-Ti chains, titania nanoclusters, etc.): the possibility to form dimeric or multimeric Ti species has been proven in Ti/SiO_2 catalysts, where supported complexes containing multiple Ti atoms exhibited catalytic acitvity in partial oxidation reactions like isolated tetrahedral Ti centers.[33–35,38] The role of these Ti species in propylene epoxidation reaction is hardly debated in the literature and a unique interpretation is absent. In particular, Song et al.[60] considered the catalytic properties of $TS\text{-}1/SiO_2$ extrudates in propylene epoxidation and they found that, upon increase of non-framework Ti species, the selectivity of propylene oxide (PO) slightly decreased, while the conversion of H_2O_2 slightly increased. Su et al.[58] focused their attention on amorphous non-framework (NFW) Ti species that severely decreased the catalytic performance of TS-1 by causing by-products formation and H_2O_2 decomposition. They found that sulfosalt impregnation method reduces the negative effects of the amorphous Ti species because of the inhibition of the acidity by metal ions such as Na^+, K^+, and the inactivation of the H_2O_2 decomposition capability of the NFW Ti species by the SO_4^{2-} ion. More recently, Zuo et al.[59] claimed that pentacoordinated Ti sites are more active than tetrahedral in HPPO. In detail, they showed as treatment with tetrapropylammonium hydroxide can improve the catalytic performance of TS-1, partly due to the formation of pentacoordinated Ti.

The different catalytic behaviors of the various Ti species most probably relates to the diverse interaction they establish with H_2O_2, finally leading to a modified catalytic cycle. The case of perfect tetrahedral sites has been deeply investigated:[57,64–66] in a very crude description, H_2O_2 first adsorbs over the Ti sites generating a Ti-peroxo or a Ti-hydroperoxo (depending on the level of hydration) species, involving the hydrolysis of a Ti-O-Si bond as well. Similar mechanisms have been inferred also in the case of tripodal Ti sites, where the bare Ti site already miss a linkage with the framework, thus exposing a titanol group. Then, the Ti-(hydro)peroxo reacts with propylene, transferring an oxygen atom to its double bond to form the epoxide moiety. By eliminating the residual water molecule, the Ti site is restored and the catalytic cycle concludes. On the other hand, few literature works proposed catalytic cycles involving defective Ti sites. Su et al.[58] suggested as Ti defects structures like Ti-O-Ti chains, which can interact with H_2O_2 after the hydrolysis of a Ti-O-Ti (or Ti-O-Si) bond to generate a titanol group, thus forming Ti-(hydro)peroxo species fully comparable to those involving perfect Ti sites, but whose lower stability results in an increased H_2O_2 decomposition. Guo and coworkers[67] postulated an isolated octahedral defective Ti, bipodally linked to the zeolitic framewok and whose coordination sphere is completed by two titanols and two adsorbed water molecules. Such Ti center interacts with H_2O_2 forming a Ti-peroxo complex through the elimination of a titanol and an ancillary water molecule; upon contact with propylene the latter oxidizes it to propylene oxide. Alternatively, they also proposed a side reaction path leading to propylene glycol.

Besides the above considered different Lewis Ti sites, also weak Brønsted acid sites (generated by Si or Ti vacancies in the framework)[68–70] seem to have a role in HPPO reaction. In fact silanol, titanol and Ti-hydroperoxo species participate quite efficiently to the PO solvolysis (alcoholysis and hydrolysis).[71]

In the present work, three TS-1 samples, showing different amounts of all the above described Ti families and weak Brønsted acid species, are considered. A deep qualitative and quantitative characterization (by means of DR-UV-Vis, Raman, FT-IR and Ti K-edge XANES spectroscopies) of all these active sites has been performed and these results have been correlated to the catalytic activity in the HPPO process.

2. Experimental Section

2.1. Materials

Three Titanium Silicalite-1 (TS-1) samples were provided by Evonik Industries AG and fully characterized as shown in the following sections. The three materials will be hereafter referred to as TS-1A, TS-1B and TS-1C. They possess the expected MFI structure and similar crystallinity, as shown by the powder XRD patterns reported in Figure S1 of SI. Their Ti content (from ICP analysis, as provided by the producer) and the Specific Surface Areas (SSAs, derived from the N_2 adsorption isotherms at 77 K reported in Figure S2 of SI through the Langmuir and the Brunauer-Emmett-Teller (BET) models) are reported in Table 1. The main feature of the selected samples is the different Ti speciation, as will be discussed in the following. TS-1A and TS-1B materials have similar Ti contents, whereas TS-1C was synthesized with a higher Ti loading, in order to deliberately increase the number of non-perfect Ti-species. The SSA values are in agreement with the ones expected for an MFI zeolite.[72] SEM analysis of the three samples shows they are closely similar under the morphological point of view, presenting nearby spherical aggregates with diametes in the 0.5-10 μm range (see Figure S3 of SI).

Table 1. Ti loadings, as calculated by ICP analysis, and SSA (BET) for the TS-1 samples considered in this study.

Sample name	TiO_2 wt%	SSA (m^2g^{-1})	
		Langmuir	BET
TS-1A	2.44	573	430
TS-1B	2.89	663	496
TS-1C	4.33	635	476

2.2. Catalysts characterization

A multi-technique approach has been applied to the characterization of the selected TS-1 catalysts, employing Diffuse Reflectance (DR) UV-Vis spectroscopy, Raman spectroscopy (exploiting multiple laser lines) and FT-IR spectroscopy (both in transmission and ATR mode).

DR-UV-Vis spectra were collected on a Varian Cary5000 spectrophotometer, equipped with a diffuse reflectance sphere. The samples were measured in a home-made bulb quartz cell, allowing to perform thermal treatments. All the materials were measured first "as such" in air, then upon the following activation procedure: each sample was heated up to 500 °C with a ramp of 5 °C/min under vacuum (< 10^{-3} mbar); after 1 hour of outgassing at 500 °C, 50 mbar of pure O_2 were dosed in the cell and left in contact for 1 further hour in order to oxidize the residuals of organic pollutants.

ATR-IR spectra were collected directly inside the glove-box, thus avoiding the contact of the activated samples with the atmosphere, by means of a Bruker Alpha instrument, equipped with Deuterated TriGlycine Sulfate (DTGS) detector and single reflection diamond ATR accessory. ATR-FTIR spectra were collected with a resolution of 2 cm^{-1}, accumulating 32 scans. The same

fractions of sample measured in activated form by DR-UV-Vis were exploited in the ATR-FTIR measurements as well.

FT-IR spectra in transmission mode were collected accumulating 32 scans at 2 cm^{-1} resolution on a Bruker Vertex 70 spectrophotometer, equipped with a MCT cryodetector, at "beam temperature", *i.e*. the temperature reached by samples under the IR beam (around 50°C). The samples were examined in the form of self-supporting pellets mechanically protected with a pure gold envelope. Before each measurement, all samples were activated in controlled atmosphere following the procedure reported in the DR-UV-Vis section, using a home-made quartz IR cell, equipped with KBr windows and characterized by a very small optical path (*ca*. 2 mm). After the sample activation, the cell was connected to a conventional high-vacuum glass line, equipped with mechanical and turbo molecular pumps (capable of a residual pressure $p < 10^{-3}$ mbar), that allows in situ adsorption/desorption measurements of the employed molecular probe (2,4,6-trimethylpyridine - collidine).

The band deconvolution of the UV-Vis and transmission FT-IR spectra was carried out using the FIT routine by Bruker, that allows the interactive research of the best-fit to the examined experimental spectral segment on the basis of a number of spectral components imposed by the operator. All the major spectral parameters (spectral position, half-bandwidth, percent of Gaussian profile) were allowed floating freely.

Raman spectra were measured first in air, then on the activated samples (for UV excitations only). The same treatment procedure reported above for UV-Vis measurements was applied. Three different excitation lines were chosen: 1064 nm (Bruker, solid state laser), 266 nm (CryLas FQSS 266-Q2, Diode Pumped Passively Q-Switched Solid State Laser) and 244 nm (Coherent MotoFred 300C, frequency doubled Ar^+ laser). Each laser is coupled with a different

instrument: 1064 nm spectra were collected on a Bruker RFS100 Fourier-transformed Raman spectrometer. The 266 nm spectra were collected at the BL10.2-IUVS beamline at the Elettra Sicrotrone Trieste by exploiting the experimental set-up described in Ref. [73]: the scattered light is analysed by using a triple stage spectrometer (Trivista 557, Princeton Instruments) equipped with a 1800 line/mm grating and detected by an UV enhanced CCD. The 244 nm Raman was performed on a Renishaw inVia Raman Microscope spectrometer, equipped with 3600 line/mm grating and UV enhanced CCD detector.

Ti K-edge XANES spectra were collected in transmission mode at the XAFS beamline[74] of the Elettra synchrotron operating at 2 GeV with an almost uniform current of 310 mA, in the top-up mode. Spectra where collected in transmission mode using three ionization chambers; a Ti metal foil was positioned after the second ionization chamber for on-line energy calibration.[75] The photons delivered to the sample were selected from the white beam emitted by the bending magnet using a double crystal Si(111) monochromathor detuned to 50% to minimise the third harmonic contamination. The energy resolution was $\Delta E/E < 10^{-4}$, that is better than 0.5 eV at 5000 eV. XANES spectra were collected with a step of 5.0 eV in the pre-edge region (4750–4940 eV), that progressively reduces to 0.25 eV in the edge region (4965–5000 eV), and progressively increases in the post edge region that was collected till 6000 eV to guarantee an excellent evaluation of the edge jump. TS-1 samples were hosted inside home-conceived cells that allows activation at high temperature to be made in situ.[76] The heating ramp was used to activate the samples was 5 °C/min up to 450 °C in a dynamic vacuum with a residual pressure better than 10^{-3} mbar.

2.3. Catalytic tests

The catalytic tests were carried out under model conditions exploiting a continuously stirred batch reactor (Medimex/Premex autoclave able to work in liquid phase under propylene atmosphere) with powdered catalysts at 40°C and 3 bar. Initially, the powdered catalyst (1g) was charged inside the reactor within a basket attached to a gasing stirrer, then 400 g of a 1 wt% solution of MTBE (p.a. grade, used as internal standard) in methanol (p.a. grade) were introduced by means of a HPLC pump. The reactor was pressurized with propylene (99.996%) at the desired reaction pressure (3 bar) and heated up to 40°C with a heating rate of 2 C min^{-1} under continuous stirring of the basket with 1800 RPM. The amount of charged propylene was evaluated by weighing the propylene bottle before and after the admission inside the reactor. In each catalytic test around 30 g of propylene were introduced inside the reaction chamber. In the final step, around 44 g of 30 wt% aqueous H_2O_2 solution were introduced inside the reactor by means of a HPLC pump. The time zero of the reaction was taken just after the introduction of hydrogen peroxide inside the autoclave. The initial composition of the reaction mixture (expressed as molar ratios of H_2O_2 : Propylene : H_2O : Methanol) is approximately 1 : 2 : 4 : 32. Offline gas chromatography (Agilent 7890B) was used for the quantitative analysis of the reaction solution. The conversion of H_2O_2 was determined by cerimetric titration. Samples were taken for the analysis after roughly 5, 10, 20, 30, 45, 60, 90, 120 and 180 min.

3. Results and Discussion

3.1. Catalysts characterization

3.1.1. Qualification of Ti sites

The three materials considered in this study were deeply characterized in order to obtain a clear view about the speciation of their Ti sites. Thereby, optical, UV-Raman and XANES spectroscopies were applied, as reported in Figure 1.

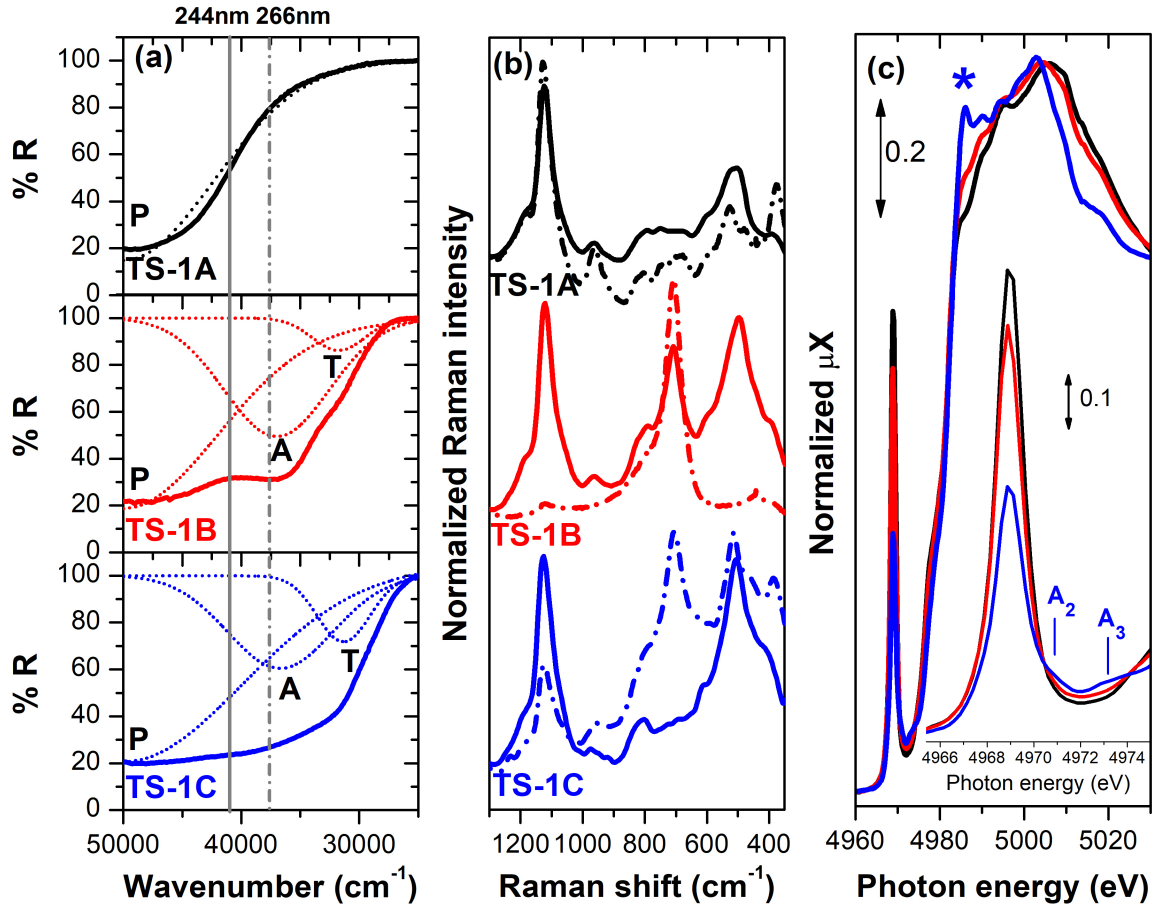

Figure 1. (a) DR-UV-Vis spectra, deconvoluted in their main spectral components (P, Perfect sites; A, Amorphous Ti sites; T; Titania); (b) UV-Raman spectra (λ = 244 nm, solid lines; λ = 266 nm, dot-dash lines); and (c) Ti K-edge XANES spectra of the three TS-1 samples. All the spectra refer to activated materials (the asterisk labels the peculiar sharp white line of the TS-1 C sample). The inset of part (c) reports a magnification of the pre-edge peak representing the fingerprint of Ti(IV) species. The UV-Raman spectra have been normalized to their most intense signal for sake of visualization. The XANES spectra have been normalized to the edge jump.

The optical spectra of Figure 1a (reported in a band resolved form to help the reader in the identification of the different spectral components) clearly depict the different nature of the three catalysts. For the sake of simplicity, the band resolution has been performed considering each component as a Gaussian peak (even if for the TiO_2 contribution an *arctg* function would have been more appropriate to describe the edge shape of the absorption) according to a methodology often exploited in the literature.[37,59] It is important to mention as these components have been deconvoluted only to facilitate the recognition of the three most important components in the optical spectrum of TS-1 samples considered in this work. Still, their meaning is barely qualitative since: i) in principle, more than a single Ti specie could contribute to the same spectral component; and ii) each electronic transition associated to a specific type of Ti structure is in principle characterized by a different extinction coefficient, *i.e.* the relative intensities of the three bands are not directly correlated to their relative amounts. In order to better evaluate the nature of the Ti sites, samples have been activated to remove every possible interaction within Ti and possible undesired adsorbates, which could affect its electronic transitions.[41] The comparison of the DR-UV-Vis spectra of all samples before and after activation are reported and commented in the SI (Figure S4a). The TS-1A sample (see black curves in Figure 1a) shows a single signal peaked at 50000 cm^{-1} (resolved component termed as P): this feature has been univocally attributed to the perfect tetrahedral framework Ti sites,[77,78] which are the only type of Ti species belonging to this sample. Considering the TS-1B material (see red curves in Figure 1a), additionally to the spectral feature proper of perfect Ti sites, a second band is revealed at 37000 cm^{-1} (resolved component termed as A). The origin of this electronic transition is still debated in the literature: in most of the cases, it has been attributed to isolated or polymerized amorphous hexacoordinated Ti species,[43,58] not incorporated into the framework. The TS-1B sample contains

a relevant fraction of such peculiar amorphous Ti species and the band width (comparable to the one of the monodispersed perfect sites) suggests that they belong to a well-defined structure. In this regard, it is worth noting that hexacoordinated Ti species forming one-dimensional …–Ti–O–Ti–O–Ti–… wires embedded in the microporous ETS-10 titanosilicate exhibit an adsorption in this region.[79,80] A further minor component is present at lower wavenumbers (resolved component termed as T), around 31500 cm^{-1}. This signal can be related to the formation of a polymorph of bulk TiO_2, whose electronic transitions fall in this spectral region.[81–83] However, on the basis of the only optical spectroscopy, the assignment of this component to a specific polymorph of titania is not straightforward. Finally, the TS-1C sample (see blue curves in Figure 1a) exhibits the larger amount of extra-framework bulk TiO_2 (as expected from its considerably large Ti loading), being decreased the amount of amorphous Ti species (A). In fact, in this case, the 31500 cm^{-1} band (T) exhibits the highest intensity along the whole set of materials. Furthermore, an almost continuous absorption is evident in the case of this sample, in the spectral range between the tetrahedral Ti-framework electronic features and the bulk TiO_2 signal. Even if the 37000 cm^{-1} component (A) is sufficient to account for it, the existence of different amorphous Ti species cannot be excluded *a priori*, since no sharp features are observed in the reflectance profile. As an example, pentacoordinated sites, expected to produce electronic transitions in the 40000-45000 cm^{-1},[59] could be present.

In order to get further insights on the different Ti species, UV-Raman spectra of activated samples were also collected (see Figure 1b). The comparison of the UV-Raman spectra of all samples before and after activation are reported and commented in Figure S4b and Figure S4c of SI. The great advantage of Raman and UV-Raman spectroscopy in TS-1 characterization arises from the possibility to selectively exploit the resonance of the different Ti species.[10,39,40,42,43,58,84,85]

Thanks to the resonance effect, some vibrational modes, associated to Ti species absorbing the excitation light, are selectively enhanced as the spectra reported in Figure 1b (compare solid-dot-dash spectra). Starting from TS-1A, the main evidences of the introduction of the Ti in tetrahedral position are found at 960 cm^{-1} and 1125 cm^{-1}, in the spectra collected with both the available excitation lasers (see solid and dash-dotted spectra in Figure 1b), respectively due to due to Ti-O-Si antisymmetric and symmetric stretching vibrations.[40,42] At lower frequency, as already described by Li et al.,[44] further absorptions, observed around 500 cm^{-1}, were assigned to modes still involving Ti(IV) in tetrahedral coordination. The Raman spectrum collected on the TS-1A sample with the 266 nm laser excitation (see the dash-dotted black spectrum in Figure 1b), with a lower resonant enhancement of the vibrational modes associated to the tetrahedral Ti sites, exhibits all the above mentioned spectral features, except for the band at 380 cm^{-1}, ascribable to the 5-membered rings typical of the MFI topology.[86,87]

For what concerns the TS-1B sample, the 244 nm Raman spectrum (see the solid red spectrum in Figure 1b) closely resembles the TS-1A one, except for the sharp signal centered at 700 cm^{-1}. By means of the 266 nm excitation laser, this latter band appears as the most intense signal of the spectrum, overcoming the perfect Ti signals by an order of magnitude. The signals of the perfect Ti sites becomes thus poorly visible, but they are still present as highlighted in Figure S5 of SI. As the excitation frequency is close to the one of the electronic transition attributed to the amorphous Ti sites, it is reasonable to attribute this band to a resonantly enhanced mode of these species. This assumption is in good agreement with the previous experimental observations,[43,58,67] even if the assignments proposed in the literature concerns different Ti structures. Since the UV-Raman spectra reported in Figure 1b have been collected after sample activation at 500 °C under high vacuum, these spectral features cannot likely be ascribed to the isolated octahedral sites

suggested by Guo et al.[67] because the ancillary water ligands considered in this model should reasonably desorb under the present activation conditions, causing a significant alteration of the related vibrational modes. Finally, the TS-1C catalyst exhibits an UV-Raman spectrum similar to TS-1A sample, employing the 244 nm excitation laser (see the solid blue spectrum in Figure 1b), whereas the spectrum collected with the 266 nm laser (see the dash-dotted blue spectrum in Figure 1b) (clearly shows an intermediate situation, in which the 700 cm^{-1} component possesses an intensity perfectly comparable to the signals generated by perfect Ti sites. According to its DR-UV-Vis spectrum (see solid blue curve in Figure 1a), the TS-1C sample is expected to be the richest of amorphous Ti sites. In fact, due to the almost continuous UV-Vis absorption of this sample in the 50000-30000 cm^{-1} range, this material probably possesses amorphous species of different nature with respect to those showed by the TS-1B sample that, even giving similar electronic transitions, are not resonantly enhanced. The resonant enhancement does not occur for these species most probably for symmetry reasons (*i.e.* the symmetry of the electronic transition does not match with the vibrational ones).[40,42]

To further validate our investigation, we exploited the element selectivity of X-ray absorption spectroscopy, collecting the XANES spectra of the three activated TS-1 samples (Figure 1c).

The $1s \rightarrow 3pd$ electronic transition in the pre-edge region of the XANES spectra of Ti(IV) minerals, glasses xerogels and materials in general is directly correlated, in both energy position and intensity, with the coordination of Ti atoms: moving from tetrahedral through penta-coordinated to octahedral Ti(IV) species, the $1s \rightarrow 3pd$ transition blue shifts by about 2 eV and loses intensity from ~ 0.8 to ~ 0.2 with respect to the edge jump. Indeed, the same electronic transition for Ti(IV) species in TiO_2 (anatase or rutile) or in ETS-10 titanosilicate, where Ti(IV) species are in octahedral environment, is characterized by a very low intensity due to the small

pd hybridisation which occurs in octahedral symmetry. The $A_{1g} \rightarrow T_{2g}$ transitions are symmetrically forbidden in the case of octahedral coordination of Ti(IV), whereas the $A_1 \rightarrow T_2$ transitions are allowed in the case of tetrahedral coordination of Ti(IV), as for [TiO_4] units hosted in the dehydrated perfect TS-1.[40,46,88,89]

The most peculiar feature of the spectra of the dehydrated TS-1A material (Fig. 1c, black curve). is indeed the narrow and intense $1s \rightarrow 3pd$ pre-edge peak at 4968.9 eV, testifying the unambiguous tetrahedral coordination of Ti(IV) species proper of perfect TS-1.[46,88,89] The XANES spectrum of sample TS-1B (red curve in Fig. 1c) exhibits the same features of that of sample TS-1A, with the only exception of a slightly less intense pre-edge peak. The intensity decrease reflects a decrease of the fraction of Ti(IV) in tetrahedral coordination, that however remains the dominant Ti species in activated TS-1B. No spectral components ascribable to the fraction of non-perfect Ti can be straightforwardly appreciated in this spectrum. The $1s \rightarrow 3pd$ peak undergoes a further intensity decrease in the XANES spectrum of activated TS-1C but, in this case, additional features are observed. In the spectral region between the pre-edge and the edge (4970–4975 eV), two very weak features appeared (indicated as A_2 and A_3 in the inset of Figure 1c): these are the fingerprints of a bulk TiO_2 phase.[88,90,91] A third, low energy peak (labeled as A_1) of bulk TiO_2 phase escapes detection, because overshadowed by the most intense peak due to the tetrahedral fraction of Ti(IV). The latter feature probably causes the significant broadening of the $1s \rightarrow 3pd$ peak (see the FWHM reported in Table 2), together with a larger heterogeneity of the tetrahedral Ti(IV) species.

Table 2. Position, intensity and full width at half maximum (FWHM) of the XANES $1s \rightarrow 3pd$ electronic transition involving Ti(IV) atoms in tetrahedral coordination in the three samples. The last column reports the evaluation of fraction of tetrahedral Ti(IV) in TS-1 A, TS-1B and TS-1C estimated from the intensity of the $1s \rightarrow 3pd$ transition, vide infra section 3.1.2.

Sample	wt% TiO_2 tot	Peak position (eV)	Peak intensity	Peak FWHM (eV)
TS-1A	2.44	4968.9	0.86	1.43
TS-1B	2.89	4968.9	0.74	1.47
TS-1C	4.33	4968.9	0.45	1.65

3.1.2 Quantification of Ti sites

DR-UV-Vis and UV-Raman spectroscopies were employed to qualitatively assess the speciation of titanium in the three catalysts. In order to move toward a more quantitative description of the TS-1 sites, a combined ATR-IR and FT-Raman (λ = 1064 nm) approach was adopted: in particular, the former was exploited to quantify the framework content of perfect tetrahedral Ti centres, whereas the latter is the most suitable in the bulk titania quantification. The use of a Raman excitation wavelength far away from any electronic absorption of the materials guarantees the absence of resonance effects.[10,39,40,42,43,58,67,85] Thereby, the intensity of each signal directly relates to the concentration of the corresponding chemical moiety.

The direct proportionality between the spectral intensity of the FTIR 960 cm^{-1} band and the framework Ti content has been proven since long time.[1,40] A possible source of error is represented by the overlap of this band with the signals arising from: i) the Si–O stretching mode of silanol groups; and ii) the stretching modes of double Si–O–Si bonds between the same pair of adjacent Si formed upon thermal elimination of adjacent silanols.[40,69,70,92] However, this contribution is expected to be small, since the intensity of these mode is poor compared to the

absorption generated by the Ti insertion, even in SiOH rich materials as silicas and defective silicalites.[86] Additionally, the insertion of Ti reduces the number of silanol nests,[93] thus decreasing the extent of the possible quantification error. For all these reasons, the contribution deriving from the stretching modes of Si–O in silanols and/or strained Si–O–Si bonds formed during thermal activation by hydroxyl elimination in adjacent SiOH groups can be neglected. In order to corroborate this assumption, the ATR-IR spectrum of an activated TS-1 sample (TS-1A) has been compared in Figure S6b of the SI with the spectrum of a pure defective silicalite containing a similar silanols population, or rather a slightly higher number of hydroxylated cavities. The normalized FT-IR spectra of the two activated samples collected in transmission mode have been also reported in the OH range (Figure S6a of the SI) to prove the similarity between the two samples in this spectral region. From this comparison, it is clear that the contribution to the 960 cm^{-1} band of stretching modes of Si–O in silanols and/or strained Si–O–Si bonds is negligible and, as a consequence, a direct proportionality between the spectral intensity of the FT-IR 960 cm^{-1} band and the framework Ti content can be considered. Furthermore, in order to perform a proper quantification, it is important to consider that any change in the coordination shell of Ti (*e.g.* the adsorption of small basic molecules) leads to a perturbation of this signal. In fact, the position of the 960 cm^{-1} band blue-shifts if the coverage increases and at the same time, its spectral intensity decreases.[41,94] For this reason, a proper activation of the material is essential to remove all the potentially adsorbed molecules and to consequently get a realistic quantification of the perfect Ti species. With respect to the past,[40] the ATR-IR spectra were preferred (see Figure 2a) to the traditional transmission FT-IR ones, thus allowing the 960 cm^{-1} band to be "in scale" employing a trivial preparation procedure. In order to keep the sample in activated conditions during the measurement, the ATR-IR spectra reported in

Figure 2a were collected directly inside the glove-box under N_2 protective atmosphere, as reported in the experimental section.

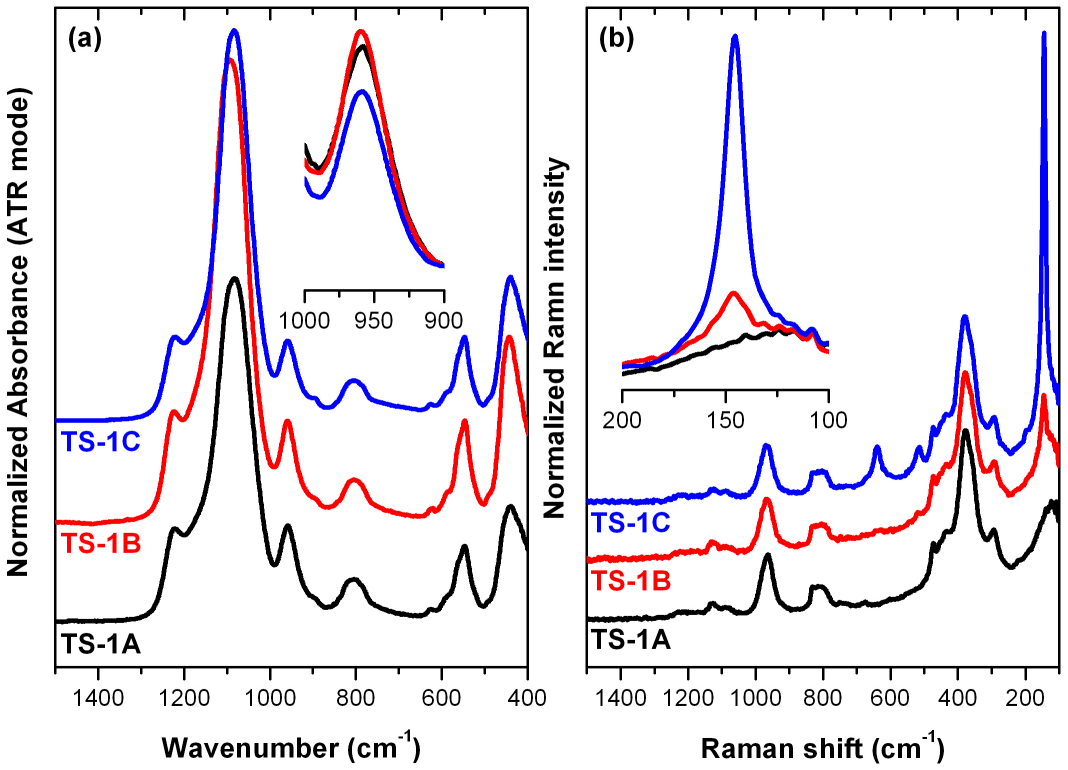

Figure 2. (a) ATR-IR and (b) FT-Raman (λ = 1064 nm) spectra of the three TS-1 samples. The ATR-IR spectra refer to samples activated at 500°C. FT-Raman ones were instead collected on the "as such" materials. For quantitative purposes, both the datasets have been normalized to the 800 cm^{-1} MFI framework mode. In the insets, a detail of the 960 cm^{-1} (ATR) and 144 cm^{-1} (FT-Raman) bands exploited for the quantifications.

By means of FT-Raman (λ = 1064 nm) spectroscopy, the amount of bulk TiO_2 was estimated too. Since the spectral vibrational modes of bulk TiO_2 should not be relevantly affected by surface adsorption, the measurements were performed on untreated samples (*i.e.* in air). Comparing the spectra of the three samples (Figure 2b), it is evident that TS-1B and TS-1C exhibit an additional sharp peak at 144 cm^{-1}, straightforwardly ascribable to the intense E_g

vibration of anatase.[95] This specific band was exploited for the anatase quantification. In order to obtain an actual quantitative information, both ATR-IR and FT-Raman spectra were normalized to the 800 cm^{-1} band (ascribed to the symmetric Si-O-Si framework stretching, thus due only to the siliceous matrix of MFI).[86] In this way, the integrated areas of the 960 cm^{-1} and 144 cm^{-1} bands can be related to the amount of tetrahedral Ti and anatase respectively. The quantification of the different Ti species was achieved exploiting the calibration curves reported in Figure 3. Data reported in Figure 3a have been collected on a series of perfect TS-1 samples, specifically synthesized by Evonik; their purity (*i.e.* absence of non-perfect species) was checked by UV-Vis (see Figure S7 of SI). Results reported in Figure 3b, instead, have been collected on a set of Silicalite-1 samples, whose crystallization gel was mixed with nano-anatase crystals (Aldrich) before hydrothermal crystallization.

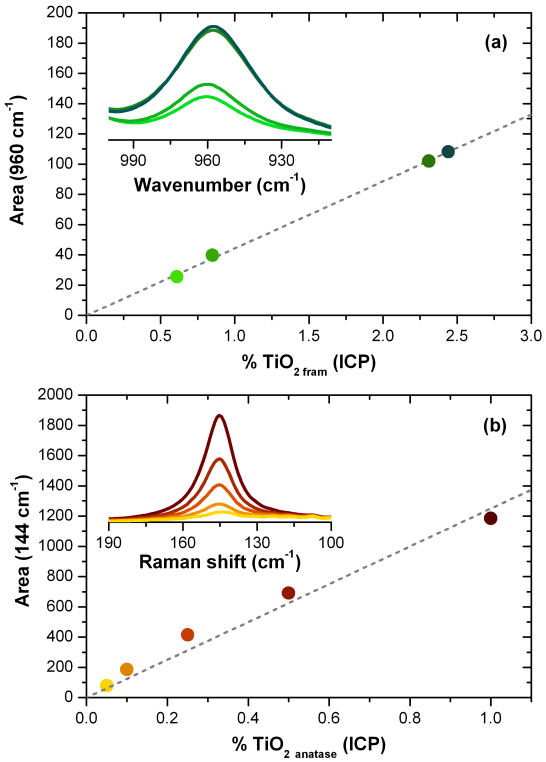

Figure 3 (a) ATR-IR calibration curve (integrated area of the 960 cm^{-1} band as a function of the total amount of in-framework Ti, as calculated by ICP analysis) for the determination of the framework Ti content; and (b) FT-Raman (λ = 1064 nm) calibration curve (integrated area of the 144 cm^{-1} band as a function of the total amount of anatase, as calculated by ICP analysis) for the determination of anatase. In the insets, the details of the 960 cm^{-1} (ATR-IR) and 144 cm^{-1} (Raman) bands exploited in the quantification are reported. All the spectra were normalized to the 800 cm^{-1} signal to ensure a quantitative comparison.

The two sets of data reported in Figure 3 refer to dedicated samples, specifically synthesized by Evonik for calibration purposes. In the case of the in-framework Ti concentration, regular TS-1 sample with only perfect Ti sites were produced with variable Ti loading. For the anatase calibration, nano-anatase particles (supplied by Sigma-Aldrich) were incorporated in the gel of a Silicalite-1 (*i.e.* purely siliceous MFI) before crystallization, thus allowing the trapping of the bulk oxide in the zeolite framework. In both the sets of reference samples, the amount of Ti was determined by ICP analysis and then correlated to the spectroscopic features. The integrated area of the 960 cm^{-1} band (whose quantitative relation with perfect Ti is well established)[1,40] was then related to the perfect Ti content, whereas the integrated area of the anatase 144 cm^{-1} Raman peak was exploited for its quantification.[95] The following linear correlations (where the intercept has been trivially set to zero) have been obtained:

$$\text{Area}\ (960\ cm^{-1}) = \text{wt\%}\ TiO_{2\ \text{perfect}} \cdot 44.289 \quad (R^2 = 0.9997) \quad (1)$$

$$\text{Area}\ (144\ cm^{-1}) = \text{wt\%}\ TiO_{2\ \text{anatase}} \cdot 1249.7 \quad (R^2 = 0.9866) \quad (2)$$

Equations 1 and 2 have been applied to the data extracted from Figure 2, allowing the Ti quantification for the three TS-1 samples investigated in this work. The results are reported in Table 3.

Table 3. Speciation of Ti sites expressed as TiO_2 wt% from combined ATR-IR and FT-Raman experiments. In brackets, the fraction of each type of site, calculated as: wt% TiO_2 site/wt% TiO_2 tot. Speciation of the relative fraction of perfect Ti from XANES is reported for comparison.

Sample	wt% TiO_2 tot	wt% TiO_2 perfect	wt% TiO_2 anatase	wt% TiO_2 amorphous	Perfect Ti XANES[a]
TS-1A	2.44	2.44 (1.00)	0.00 (0.00)	0.00 (0.00)	1.00
TS-1B	2.89	2.57 (0.89)	0.12 (0.04)	0.20 (0.07)	0.86
TS-1C	4.33	2.09 (0.48)	0.37 (0.09)	1.87 (0.43)	0.52

[a] The fraction of perfect Ti has been evaluated by dividing the intensity of the $1s \rightarrow 3pd$ pre-edge peak of each sample for the intensity of the $1s \rightarrow 3pd$ pre-edge peak of the TS-1A sample (as it contains only perfect Ti sites). Intensity values are reported in Table 2.

Clearly, knowing the total amount of Ti (as calculated by ICP analysis) and the contents of perfect Ti and anatase, the fraction of amorphous Ti can be simply derived from subtraction. It is worth mentioning that the label amorphous Ti (indicated as A in the DR-UV-Vis spectra) refers to a single type of Ti species in the TS-1B sample (according to the qualification results), whereas amorphous Ti sites of different nature are most probably present in TS-1C. As further crosscheck, the fraction of tetrahedral Ti(IV) species estimated by ATR-IR experiments has been compared with the semi-quantitative results derived from XANES. Since TS-1A contains just perfect Ti, the intensity of its $1s \rightarrow 3pd$ feature is due only to this type of Ti species. Thus, by calculating the ratio between the intensities of the pre-edge peak of TS-1B/TS-1C and the one of TS-1A, the fraction of perfect Ti in these samples can be estimated. This semi-quantification (see Table 3) is in good agreement with the ATR-IR findings: the fraction of perfect Ti for TS-1B and TS-1C samples has been evaluated to be 0.86 and 0.52 respectively. This outcome testifies the goodness of our ATR-IR-based calibration strategy.

3.1.3 FT-IR study of external and internal hydroxyl groups

After the qualitative and quantitative evaluation of the Ti centers, the hydroxyl population (both external and internal) of all the catalysts has been extensively evaluated by means of transmission FT-IR spectroscopy. Figure 4a and 4b report the spectra, in the OH stretching region, of all the samples after activation at 500°C (see black, red and blue spectra). Figure 4c, additionally, displays the differential FT-IR spectra normalized to the TS-1 overtone modes of collidine saturated samples, in the spectral region of collidine ring vibrations. As demonstrated by the extremely abundant and well-established literature on the subject (see for example ref. [69,70,96–98] and references therein), the complex envelope of bands in the 3800-3200 cm^{-1} spectral range is ascribable to the presence of both isolated and interacting OH groups (possibly both SiOH and TiOH species, characterized by very similar O-H stretching frequencies and, for this reason, not distinguishable)[99] located on the external and on the internal surface of TS-1. In particular, the spectral components in the 3800-3700 cm^{-1} range are generated by stretching modes of unperturbed or weakly perturbed OH groups, whereas the broad envelope between 3650 and 3200 cm^{-1} can be ascribed to adjacent silanols (titanols) mutually interacting via medium-strength hydrogen bonds, located inside the hydroxylated cavities (nests) generated by the presence of defects (*i.e.* one or more missing [SiO_4] unit in the framework). The chains length of these hydrogen-bonded hydroxyl groups depends obviously upon the number of missing [SiO_4] units.[69,70,97]

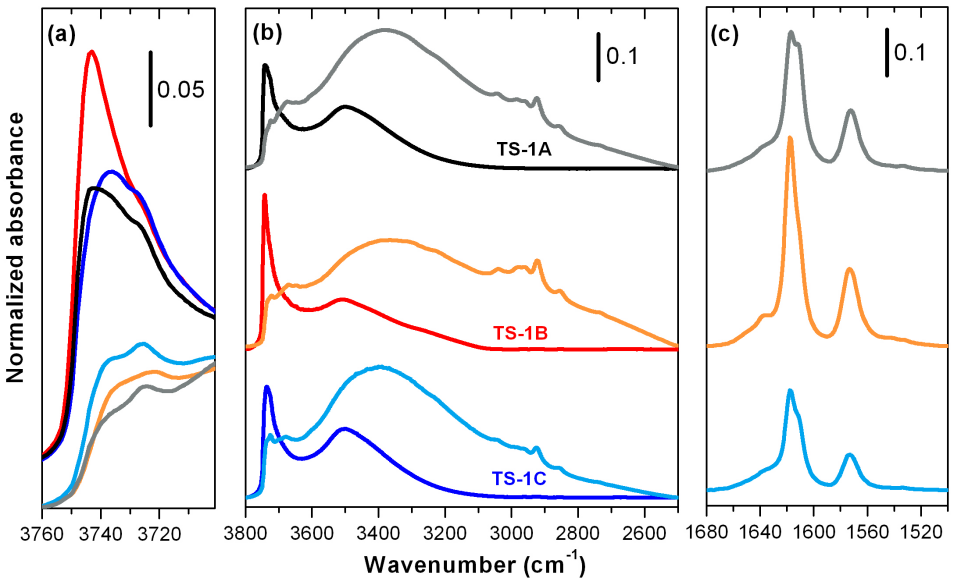

Figure 4. (a)-(b) FT-IR spectra in the OH stretching region, normalized to the TS-1 framework overtone modes, of the catalysts activated at 500°C (black-TS-1A, red-TS-1B, blue-TS-1C) and after contact with collidine vapor pressure (grey-TS-1A, orange-TS-1B, light blue-TS-1C). (c) Differential FT-IR spectra of collidine saturated samples in the ring modes spectral range of collidine. All spectra were collected at beam temperature, *i.e.* the temperature reached by the materials under the IR beam.

It is clear that the TS-1A (black spectrum) and TS-1C (blue spectrum) catalysts possess a very similar OH spectral profile with respect to sample TS-1B (red spectrum), in which the ratio between the unperturbed or weakly perturbed and the interacting hydroxyl groups is completely different. These differences are pointed out in Figure 4a, where the normalized spectra of the three activated samples (black, red and blue curves) are directly compared in the OH stretching region (ν_{OH}) of substantially unperturbed species. This apparently complex ν_{OH} envelope is actually very similar to the hydroxyls spectral profile reported in the literature for this type of defective materials for which three distinct band are usually recognized in this spectral region.[69,70] In order to study and compare the unperturbed or weakly perturbed hydroxyl

population of the catalysts, the activated samples spectra of Figure 4a were reported in a band-resolved form in Figure 5 (upper part) considering three main spectral components.

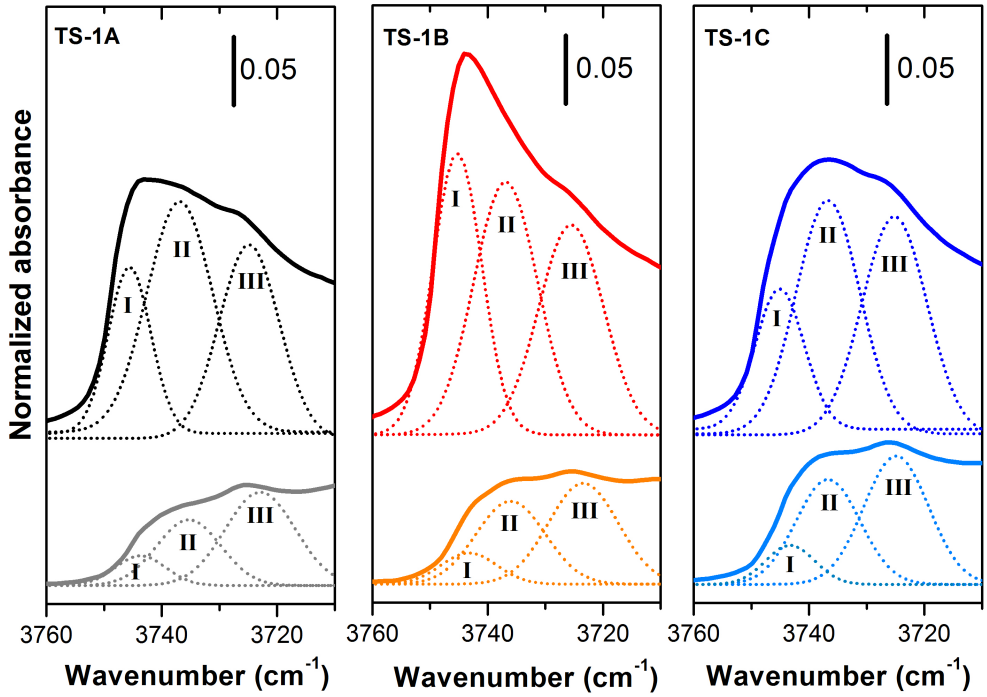

Figure 5. Band resolved FT-IR spectra in the stretching region of substantially unperturbed OH species, normalized to the TS-1 framework overtone modes, of the catalysts activated at 500°C (upper part: black-TS-1A, red-TS-1B, blue-TS-1C) and after contact with collidine vapor pressure (lower part: grey-TS-1A, orange-TS-1B, light blue-TS-1C). Full line spectra are the experimental ones, whereas dotted traces represent the resolved components, referred to as I, II and III.

The three resolved components, hereafter referred to as I, II and III, are located at 3745, 3736 and 3724 cm^{-1} respectively. The band at 3745 cm^{-1} (I) can be ascribed to fully isolated (unperturbed) SiOH (TiOH) groups, whereas the two components at 3736 (II) and 3724 (III) cm^{-1} are generated by substantially unperturbed hydroxyls groups in terminal position in hydrogen-bonded silanol chains as depicted in Scheme 1. The existence of different spectral components due to terminal OH species can be reasonably explained considering chains of mutually interacting OH groups of different length. In fact, the spectral position of the OH stretching

mode of terminal groups depends upon the chain length of the hydroxyl species interacting *via* hydrogen bond: in particular, the higher the chain length, the lower the OH stretching frequency.[69]

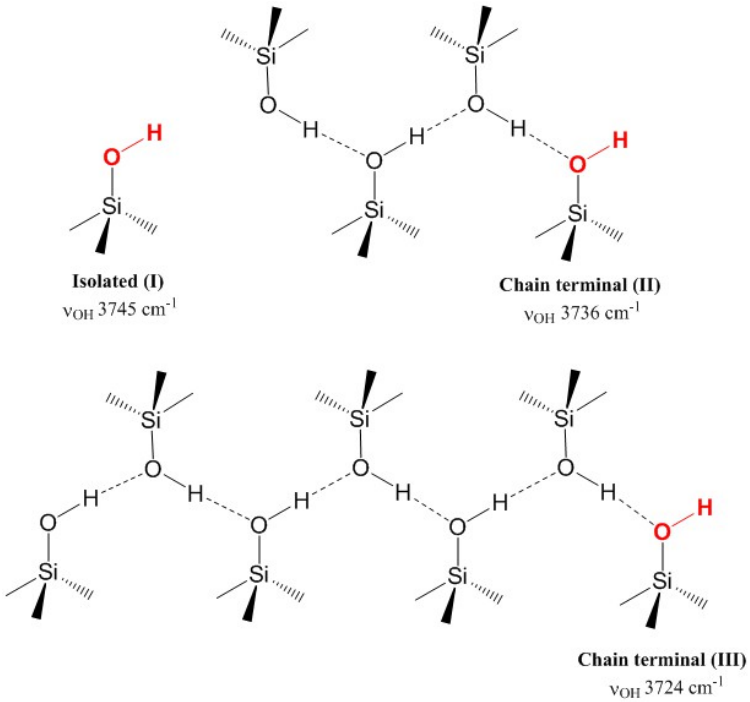

Scheme 1. Pictorial description of an isolated silanol and of terminal OH groups in chains of mutually interacting silanols of different length.

The resolved spectral components of the three activated samples shown in Figure 5 and the corresponding integrated absorbance (Area) reported in Table 4 and Table S1 highlight that, as mentioned in the discussion of Figure 4, samples TS-1A and TS-1C are characterized by a very similar OH population. In contrast, the TS-1B catalyst possesses a higher amount of isolated OH groups (see the Area of component I in Table S1) but a very similar population of weakly perturbed terminal species with respect to the other two materials (see the Area of components II+III in Tables S1 and 4). Still, in the case of samples TS-1A and TS-1C, the envelope between

3650 and 3200 cm^{-1} (see black and blue spectra in Figure 4b), due to the stretching vibration of interacting OH groups inside the nests, is definitely more intense. It probably means that both TS-1A and TS-1C catalysts are characterized by defects in which more adjacent tetrahedral [SiO_4] units are simultaneously missing and, therefore, their hydroxylated cavities contain longer chains of mutually interacting silanols closed in a loop.[68,69,97] Nevertheless, regardless of the interacting OH chains length, the population of terminals OH groups in open chains of the three samples is substantially the same (see Table 4). The different concentration of hydrogen-bonded species of these materials has probably no relevance, in fact, mainly isolated and terminals species, with a higher acidic character, can possibly affect the catalytic performances of the material.

Table 4. Integrated absorbance (Area) of the resolved spectral components I, II and III reported in Figure 5 evaluated after activation (internal + external fraction) and after contact with collidine vapors (internal fraction), relative to the total isolated-terminals OH species (I+II+III) and to the terminal (II+III) OH groups. The external SiOH/TiOH fraction, calculated by difference, is reported for completeness.

Sample	Silanol location	Area (I+II+III) (isolated & total terminals)	Area (II+III) (total terminals)
TS-1A (activated)	Internal + external	5.96	4.72
TS-1B (activated)	Internal + external	7.68	5.25
TS-1C (activated)	Internal + external	6.34	5.13
TS-1A (collidine)	Internal	2.17	1.90
TS-1B (collidine)	Internal	2.56	2.25
TS-1C (collidine)	Internal	2.99	2.65
TS-1A (difference)	External	3.79	2.82
TS-1B (difference)	External	5.12	3.00
TS-1C (difference)	External	3.35	2.48

Another important feature to consider in the characterization step of these materials is the evaluation of the substantially unperturbed hydroxyl fraction actually located on the internal surface of the TS-1 micro-channels, to understand if the presence of these weak acid centers play a role in the catalytic activity of these systems and, especially, in the by-products formation. The discrimination between internal and external OH groups is possible by performing the FT-IR study of the adsorption of a sterically hindered probe molecule, the 2,4,6-trimethylpyridine (collidine).[100,101] This basic probe, due to its diameter (7.4 Å), is too large to enter inside the MFI micropores of TS-1 and, therefore, can only interact with the acid sites fraction present at the external surface. In other words, if a silanol stretching band is affected by the adsorption of collidine, it means that the corresponding hydroxyl fraction is located outside the micro channels.

Collidine vapors were put in contact with the pre-treated samples in the FT-IR cell at room temperature (see Figure 4c). The bands at 1617 and 1572 cm^{-1} represent collidine adsorbed on Si-OH sites.[100] Consistently with results described in Figure 4a, TS-1B shows the most intense signals from collidine ring modes due probably to the larger amount of external OH species of this material that leads to the adsorption of a larger amount of probe molecule.

Figure 4b reports the normalized spectra, in the OH stretching region, of all the activated samples after contact with collidine vapour pressure (see grey, orange and light blue spectra). Consequently to the collidine interaction, it is possible to observe a strong reduction of all hydroxyl bands in the 3800-3700 cm^{-1} spectral range, consistent with the fact that the probe interacts with the isolated and the chain terminals hydroxyl groups located at the external surface, and the appearance of a broad signal in the 3600-3100 cm^{-1} region generated by the OH species interacting with the probe molecule and overlapped to the bands of perturbed silanols

located inside the TS-1 nests. The decrease of the substantially unperturbed hydroxyls signals is well evident in Figure 4a, where the normalized spectra of the three activated samples (black, red and blue curves) are directly compared with the spectra of the materials after collidine adsorption. These spectra were reported in a band resolved form (components I, II and III) in Figure 5 (lower part); in order to evaluate the internal OH population, in fact, the virtually unaffected bands imply that the corresponding OH species are located inside the microporous structure. The integrated absorbances (Area) relative to the fraction of internal hydroxyls are listed in Tables S1 and 4. The external SiOH/TiOH population was also calculated by difference and reported for completeness in Table S1 and 4. In general, the amount of isolated and terminals SiOH groups that is able to interact with collidine, *i.e.* that is located at the external surface, is around 60% of the total population. It is worth noting that sample TS-1B possesses the higher fraction of external OH population, as previously highlighted in the description of Figure 4a and 4c. Observing the Area (I+II+III) values calculated after collidine adsorption of Table 4, it is evident that the three samples contain a different amount of weakly acid internal OH species (isolated and teminals) that follows this trend: TS-1C > TS-1B > TS-1A. Moreover, from the band-resolved spectra of Figure 5, it is possible to highlight that, for all samples, the spectral component ascribed to isolated OH groups (I, 3745 cm^{-1}) is mainly eroded upon collidine dosage, because these species are mainly located at the external surface. In addition, the amount of internal isolated OH groups is essentially the same in the three samples (see the Area of component I after collidine adsorption in Table S1) and, as a consequence, the amount of internal terminals OH groups follows the above reported trend (TS-1C > TS-1B > TS-1A).

3.2 Catalytic test measurements

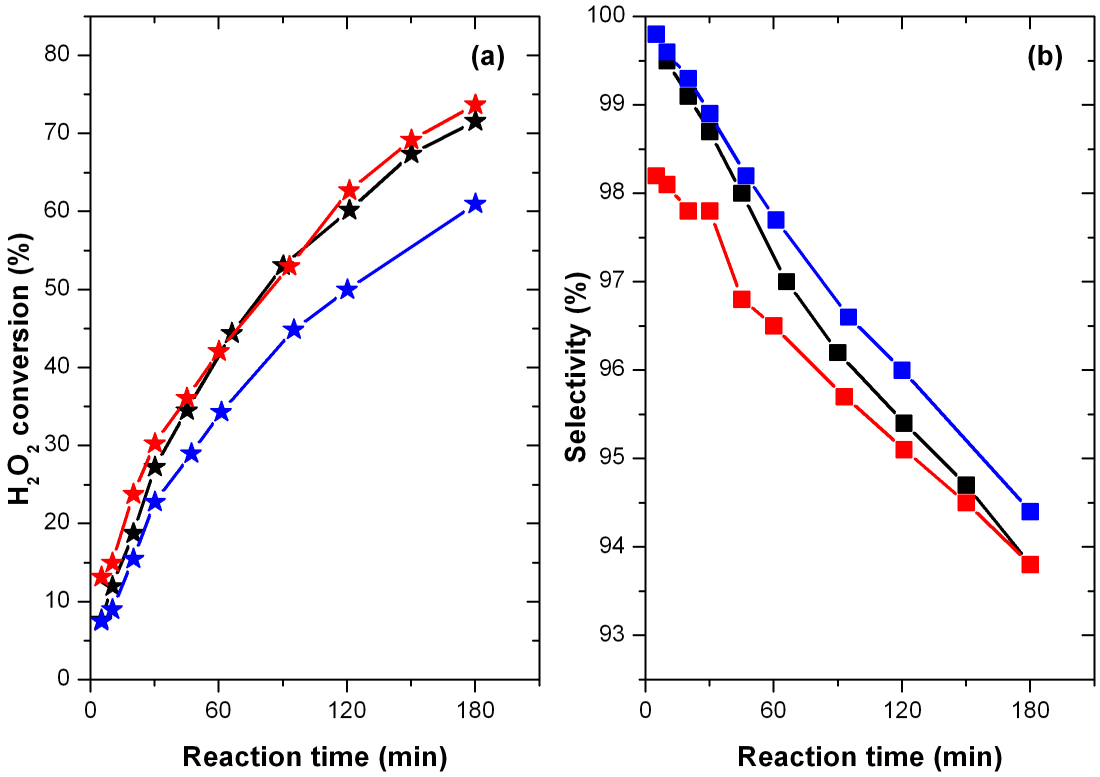

Figure 6. Catalytic data for the HPPO reaction obtained at 40 °C and 3 bar. TS-1A (black curves), TS-1B (red curves) and TS-1C (blue curves). In the panels: (a) H_2O_2 conversion (★); and (b) PO selectivity (■).

The three materials were tested as catalysts in the HPPO reaction at 40°C and 3 bar for 180 min in order to investigate a possible structure-activity relationship with respect to the nature of the various Ti species. All the catalytic results are reported in Figure 6. The catalytic tests proved that all the samples are considerably active toward the propene epoxidation reaction, however it is evident that minor differences can be highlighted. After 180 min of reaction, the conversion of H_2O_2 is very high reaching roughly 70% for both samples TS-1A and TS-1B. A slightly lower value is achieved in the presence of TS-1C, with a conversion of around 60% at 180 min. The

PO selectivity after the same reaction time is very high (around 94%) for all the catalysts. All these catalytic parameters are listed in Table 5.

Table 5. Hydrogen peroxide conversion ($\chi_{H_2O_2}$), propylene oxide selectivity (S_{PO}), by-products yields (Y_{BY}), productivity and Turnover Numbers (TON) for PO production calculated for the three samples in the HPPO reaction performed at 40 °C and 3 bar. The amounts of both total and perfect Ti centers, expressed as mg of TiO_2, are reported as well.

Sample	Catalyst amount (g)	TiO_2 tot (mg)	$\chi_{H_2O_2}$ [a] (%)	S_{PO} [a] (%)	Y_{BY} [b] (%)	Productivity [c] ($g_{PO}g_{cat}^{-1}$)	TON_{tot} [c] ($mol_{PO}mol_{TiO_2\,tot}^{-1}$)	TON_{perf} [c] ($mol_{PO}mol_{TiO_2\,perf}^{-1}$)
TS-1A	1.083	26.4	71.6	93.8	1.8	8.0	450	450
TS-1B	1.013	29.3	73.7	93.8	2.0	8.1	384	431
TS-1C	1.012	43.8	61.0	94.4	2.0	7.2	229	476

[a] after 3 h of reaction
[b] computed at 50% H_2O_2 conversion
[c] computed at 30 min of reaction

The catalytic parameters are in line with the results reported in the literature concerning experiments carried out in similar conditions.[59,67,102]

The productivity of the catalyst, expressed as g of PO produced per g of catalyst along 1 h of reaction, was computed. The obtained data show as TS-1A and TS-1B exhibit a similar behaviour, whereas TS-1C has poorer performances. This trend readily suggests that, most probably, TS-1C owns a lower number of active sites. Even if these values are meaningful for industrial application, they do not clearly allow the role of Ti species toward catalysis to be understood. Thereby, Turnover Numbers (TONs) after 30 min of reaction was calculated by considering the molar ratio between the produced PO and the amount of catalyst active sites. In this specific case, assuming that the plain siliceous matrix of TS-1 is not active in propylene epoxidation, TON calculations have been performed considering: i) the total TiO_2; or ii) the only perfect TiO_2 contents. Assuming that all the Ti sites are active (regardless of their nature), the

TON for the three catalysts is theoretically are expected to be equal. In contrast, the calculated TONs (see Table 5) reveal a higher value for TS-1A, a slightly lower one for TS-1B, whereas TS-1C presents a much lower TON. This conflicting behaviour proves that not all the Ti sites are catalytically active in the HPPO reaction. Interestingly, the TON seems to be related to the perfect Ti content only, since similar values are obtained among the three catalysts as this specific sites fraction is considered in the calculations. Therefore, the amorphous Ti species and the bulk anatase, observed in TS-1B and TS-1C catalysts, act most probably just as spectators in the H_2O_2 conversion, but considerably decreasing the fraction of available active sites with respect to the whole Ti content.

If the nature of the Ti species seems to be a secondary factor in determining the H_2O_2 conversion, it could play a role with respect to the formation of by-products. The main by-products observed in HPPO reaction generate from alcholysis and hydrolysis of PO, giving methyl esters and propylene glycol.[103] The yields of by-products, evaluated at 50% of H_2O_2 conversion and reported in Table 5, show slight differences for the three catalysts. In particular, TS-1A forms a lower amount of undesired products, suggesting that amorphous species and/or anatase present in TS-1B and TS-1C could play a role in the PO degradation.

As reported in the literature,[71] other acid functionalities could affect the catalyst selectivity as well, *i.e.* silanols and/or titanols. Comparing the data reported in Table 4 and the by-product yields given in Table 5, a relation between the amount of internal OH groups and the by-products formation could be qualitatively inferred as did previously for non-perfect Ti species. The PO degradation capacity of the catalyst is most probably weakly correlated with the internal OH population of the material: the lower the internal OH population, the lower the amount of by-products (see Area (I+II+III) reported in Table 4). Conversely, there is not a clear correlation

between the total amount of SiOH/TiOH sites (internal + external, both isolated and/or interacting) and the by-products yield, thereby the effect of the external groups cannot be clearly stated.

As a general and final comment, it is worth mentioning that all the above reported differences are rather small and, practically speaking, the behaviour of the three catalysts is almost the same at the considered reaction conditions. Future dedicated PO degradation experiments (other than regular catalytic tests) are thus necessary to fully elucidate the role of non-perfect Ti sites and of other acid functionalities (SiOH/TiOH) in by-products generation.

4. Conclusions

Three TS-1 samples with different amount and different speciation of Ti sites were fully characterized by means of different spectroscopic techniques. DR-UV-Vis, UV-Raman (λ= 244 nm and 266 nm) and Ti K-edge XANES spectroscopies showed the clear presence of both perfect tetrahedral Ti and non-perfect (amorphous hexacoordinated and/or pentacoordinated Ti and anatase) Ti species. ATR-IR, FT-Raman (λ = 1064 nm) and XANES were instead employed to perform the quantification of the recognized Ti species.

FT-IR spectroscopy proved that the three samples are characterized by a different population in weak Brønsted acid sites (hydroxy groups in silanols and titanols). The speciation and the quantification of internal *vs*. external hydroxyls were performed by means of collidine IR adsorption.

The catalytic testing of the three materials proved that non-perfect Ti species do not affect H_2O_2 conversion. Furthermore, the catalytic activity is quantitatively correlated to the perfect Ti content of each catalyst. Considering the by-products formation, non-perfect Ti species are most

probably poorly active in the PO degradation, In the same way, only a weak qualitative correlation among silanols and/or titanols and the by-products yield was found.

As a general remark, this work establishes for the first time a bridge between an extensive characterization step (also quantitative with respect to the possible active species) and the catalytic performances of the TS-1 in HPPO reaction, demonstrating the importance of a combined approach in determining the structure-property relationship in the heterogeneous catalysis field.

Supporting Information (SI)

Powder XRD patterns of the samples (Figure S1); N_2 adsorption/desoprtion isotherms at 77 K of the samples (Figure S2); SEM images of the samples (Figure S3); comparison of the optical and UV-Raman spectra of samples before and after activation (Figure S4); UV-Raman spectra (266 nm) of samples TS-1A and TS-1B highlighting the features of perfect Ti sites in the latter (Figure S5); FT-IR spectra of sample TS-1A and a pure defective silicalite, compared in their OH stretching region and nearby the 960 cm^{-1} band (Figure S6); DR-UV-Vis spectra of the perfect Ti calibration TS-1 samples (Figure S7); integrated absorbance for the single components of FT-IR band resolution, for both activated and collidine-contacted materials (Table S1). The Supporting Information is available free of charge on the ACS Publications website.

Acknowledgments

This work is part of the MS Ph.D thesis. The authors thank Evonik Resource Efficiency for the lively support to this research. We are indebted to G. Aquilanti, L. Olivi (Elettra synchrotron) and L. Braglia (CNR-IOM, Trieste) for the friendly and highly professional support during the Ti K-edge XANES experiments at the XAFS beamline of the Elettra synchrotron. CL acknowledge the Mega-grant of the Russian Federation Government to support scientific research at Southern Federal University, No. 14.Y26.31.0001. The authors acknowledge the CERIC-ERIC Consortium for the access to experimental facilities and financial support.

References

(1) Notari, B.; Perego, G.; Taramasso, M. Preparation of Porous Crystalline Synthetic Material Comprised of Silicon and Titanium Oxides. US4410501 A, 1983.

(2) Notari, B. Microporous Crystalline Titanium Silicates. In *Advances in Catalysis*; Eley, D. D., Haag, W. O., Gates, B., Eds.; Elsevier Academic Press Inc: San Diego, 1996; Vol. 41, pp 253–334.

(3) Romano, U.; Ricci, M. Industrial Applications. In *Liquid Phase Oxidation via Heterogeneous Catalysis*; Clerici, M. G., Kholdeeva, O. A., Eds.; John Wiley & Sons, Inc.: Hoboken, New Jersey, 2013; pp 451–506.

(4) Russo, V.; Tesser, R.; Santacesaria, E.; Di Serio, M. Chemical and Technical Aspects of Propene Oxide Production via Hydrogen Peroxide (HPPO Process). *Ind. Eng. Chem. Res.* **2013**, *52*, 1168–1178.

(5) Lin, M.; Xia, C.; Zhu, B.; Li, H.; Shu, X. Green and Efficient Epoxidation of Propylene

with Hydrogen Peroxide (HPPO Process) Catalyzed by Hollow TS-1 Zeolite: A 1.0 Kt/a Pilot-Scale Study. *Chem. Eng. J.* **2016**, *295*, 370–375.

(6) Schmidt, F.; Bernhard, M.; Morell, H.; Pascaly, M. HPPO Process Technology A Novel Route to Propylene Oxide without Coproducts. *Chem. Today* **2014**, *32*, 31–35.

(7) Adedigba, A. L.; Sankar, G.; Catlow, C. R.; Du, Y.; Xi, S.; Borgna, A. On the Synthesis and Performance of Hierarchical Nanoporous TS-1 Catalysts. *Microporous Mesoporous Mater.* **2017**, *244*, 83–92.

(8) Nguyen, H. K. D.; Sankar, G.; Catlow, R. A. Reactivities Study of Titanium Sites in Titanosilicate Frameworks by in Situ XANES. *J. Porous Mater.* **2017**, *24*, 421–428.

(9) Welch, A.; Shiju, N. R.; Watts, I. D.; Sankar, G.; Nikitenko, S.; Bras, W. Epoxidation of Cyclohexene over Crystalline and Amorphous Titanosilicate Catalysts. *Catal. Letters* **2005**, *105*, 179–182.

(10) Xiong, G.; Cao, Y.; Guo, Z.; Jia, Q.; Tian, F.; Liu, L. The Roles of Different Titanium Species in TS-1 Zeolite in Propylene Epoxidation Studied by in Situ UV Raman Spectroscopy. *Phys. Chem. Chem. Phys.* **2016**, *18*, 190–196.

(11) Zuo, Y.; Liu, M.; Ma, M.; Song, C.; Guo, X. Improved Catalytic Performance for 1-Butene Epoxidation over Titanium Silicalite-1 Extrudates by Using SBA-15 or Carborundum as Additives. *Ind. Eng. Chem. Res.* **2017**, *56*, 7462–7467.

(12) Adam, W.; Corma, A.; Indrasena Reddy, T.; Renz, M. Diastereoselective Catalytic Epoxidation of Chiral Allylic Alcohols by the TS-1 and Ti-β Zeolites: Evidence for a Hydrogen-Bonded, Peroxy-Type Loaded Complex as Oxidizing Species. *J. Org. Chem.* **1997**, *62*, 3631–3637.

(13) Van Der Waal, J. C.; Rigutto, M. S.; Van Bekkum, H. Zeolite Titanium Beta as a

Selective Catalyst in the Epoxidation of Bulky Alkenes. *Appl. Catal. A Gen.* **1998**, *167*, 331–342.

(14) Davies, L. J.; McMorn, P.; Bethell, D.; Page, P. C. B.; King, F.; Hancock, F. E.; Hutchings, G. J. Epoxidation of Crotyl Alcohol Using Ti-Containing Heterogeneous Catalysts: Comments on the Loss of Ti by Leaching. *J. Catal.* **2001**, *198*, 319–327.

(15) Kerton, O. J.; McMorn, P.; Bethell, D.; King, F.; Hancock, F.; Burrows, A.; Kiely, C. J.; Ellwood, S.; Hutchings, G. Effect of Structure of the Redox Molecular Sieve TS-1 on the Oxidation of Phenol, Crotyl Alcohol and Norbornylene. *Phys. Chem. Chem. Phys.* **2005**, *7*, 2671–2678.

(16) Wróblewska, A.; Rzepkowska, M.; Milchert, E. Epoxidation of Methallyl Alcohol with Hydrogen Peroxide over TS-1 Catalyst. *Appl. Catal. A Gen.* **2005**, *294*, 244–250.

(17) Wróblewska, A.; Wajzberg, J.; Milchert, E. Epoxidation of 1-Butene-3-Ol with Hydrogen Peroxide under Autogenic and Atmospheric Pressure. *J. Adv. Oxid. Technol.* **2007**, *10*, 316–324.

(18) Wróblewska, A. The Epoxidation of Limonene over the TS-1 and Ti-SBA-15 Catalysts. *Molecules* **2014**, *19*, 19907–19922.

(19) Wang, W.; Fu, Y.; Guo, Y. Y.; Guo, Y. Y.; Gong, X. Q.; Lu, G. Preparation of Lamellar-Stacked TS-1 and Its Catalytic Performance for the Ammoximation of Butanone with H_2O_2. *J. Mater. Sci.* **2017**, *53*, 1–12.

(20) Alba-Rubio, A. C.; Fierro, J. L. G.; León-Reina, L.; Mariscal, R.; Dumesic, J. A.; López Granados, M. Oxidation of Furfural in Aqueous H_2O_2 Catalysed by Titanium Silicalite: Deactivation Processes and Role of Extraframework Ti Oxides. *Appl. Catal. B Environ.* **2017**, *202*, 269–280.

(21) Horwitz, C. P. Oxidation Catalysts Green Oxidation Catalyst for Green Chemistry Green Chemistry. In *Encyclopedia of Sustainability Science and Technology*; Springer New York: New York, NY, 2012; pp 7585–7618.

(22) Serrano, D.; Sanz, R.; Pizarro, P.; Moreno, I. Turning TS-1 Zeolite into a Highly Active Catalyst for Olefin Epoxidation with Organic Hydroperoxides. *Chem. Commun.* **2009**, *11*, 1407–1409.

(23) Cheneviere, Y.; Chieux, F.; Caps, V.; Tuel, A. Synthesis and Catalytic Properties of TS-1 with Mesoporous/microporous Hierarchical Structures Obtained in the Presence of Amphiphilic Organosilanes. *J. Catal.* **2010**, *269*, 161–168.

(24) Tsai, S.-T.; Chao, P.-Y.; Tsai, T.-C.; Wang, I.; Liu, X.; Guo, X.-W. Effects of Pore Structure of Post-Treated TS-1 on Phenol Hydroxylation. *Catal. Today* **2010**, *148*, 174–178.

(25) Serrano, D. P.; Sanz, R.; Pizarro, P.; Moreno, I. Tailoring the Properties of Hierarchical TS-1 Zeolite Synthesized from Silanized Protozeolitic Units. *Appl. Catal. A Gen.* **2012**, *435–436*, 32–42.

(26) Moreno, I.; Dummer, N. F.; Edwards, J. K.; Alhumaimess, M.; Sankar, M.; Sanz, R.; Pizarro, P.; Serrano, D. P.; Hutchings, G. J. Selective Oxidation of Benzyl Alcohol Using in Situ Generated H_2O_2 over Hierarchical Au-Pd Titanium Silicalite Catalysts. *Catal. Sci. Technol.* **2013**, *3*, 2425–2434.

(27) Cheng, W.; Jiang, Y.; Xu, X.; Wang, Y.; Lin, K.; Pescarmona, P. P. Easily Recoverable Titanosilicate Zeolite Beads with Hierarchical Porosity: Preparation and Application as Oxidation Catalysts. *J. Catal.* **2016**, *333*, 139–148.

(28) Serrano, D. P.; Sanz, R.; Pizarro, P.; Moreno, I. Synthesis of Hierarchical TS-1 Zeolite

from Silanized Seeds. *Top. Catal.* **2010**, *53*, 1319–1329.

(29) Sanz, R.; Serrano, D. P.; Pizarro, P.; Moreno, I. Hierarchical TS-1 Zeolite Synthesized from SiO_2-TiO_2 Xerogels Imprinted with Silanized Protozeolitic Units. *Chem. Eng. J.* **2011**, *171*, 1428–1438.

(30) Serrano, D. P.; Sanz, R.; Pizarro, P.; Moreno, I.; Shami, S. Narrowing the Mesopore Size Distribution in Hierarchical TS-1 Zeolite by Surfactant-Assisted Reorganization. *Microporous Mesoporous Mater.* **2014**, *189*, 71–82.

(31) Lin, K.; Li, L.; Sels, B. F.; Jacobs, P. A.; Pescarmona, P. P. Titanosilicate Beads as Versatile Catalysts for the Conversion of Trioses to Lactates and for the Epoxidation of Alkenes. *Catal. Today* **2011**, *173*, 89–94.

(32) Chen, L.-H.; Li, X.-Y.; Tian, G.; Li, Y.; Rooke, J. C.; Zhu, G.-S.; Qiu, S.-L.; Yang, X.-Y.; Su, B.-L. Highly Stable and Reusable Multimodal Zeolite TS-1 Based Catalysts with Hierarchically Interconnected Three-Level Micro-Meso-Macroporous Structure. *Angew. Chem. Int. Ed.* **2011**, *50*, 11156–11161.

(33) Kholdeeva, O. A.; Ivanchikova, I. D.; Guidotti, M.; Pirovano, C.; Ravasio, N.; Barmatova, M. V.; Chesalov, Y. A. Highly Selective Oxidation of Alkylphenols to Benzoquinones with Hydrogen Peroxide over Silica-Supported Titanium Catalysts: Titanium Cluster Site versus Titanium Single Site. *Adv. Synth. Catal.* **2009**, *351*, 1877–1889.

(34) Kholdeeva, O. A.; Ivanchikova, I. D.; Guidotti, M.; Ravasio, N.; Sgobba, M.; Barmatova, M. V. How to Reach 100% Selectivity in H_2O_2-Based Oxidation of 2,3,6-Trimethylphenol to Trimethyl-P-Benzoquinone over Ti,Si-Catalysts. *Catal. Today* **2009**, *141*, 330–336.

(35) Carniato, F.; Bisio, C.; Sordelli, L.; Gavrilova, E.; Guidotti, M. Ti-POSS Covalently Immobilized onto Mesoporous Silica: A Model for Active Sites in Heterogeneous

Catalytic Epoxidation. *Inorganica Chim. Acta* **2012**, *380*, 244–251.

(36) Wang, W.; Fu, Y.; Guo, Y.; Guo, Y.; Gong, X. Q.; Lu, G. Preparation of Lamellar-Stacked TS-1 and Its Catalytic Performance for the Ammoximation of Butanone with H_2O_2. *J. Mater. Sci.* **2018**, *53*, 4034–4045.

(37) Zuo, Y.; Wang, X.; Guo, X. Synthesis of Titanium Silicalite-1 with Small Crystal Size by Using Mother Liquid of Titanium Silicalite-1 As Seed. *Ind. Eng. Chem. Res.* **2011**, *50*, 8485–8491.

(38) Brutchey, R. L.; Mork, B. V.; Sirbuly, D. J.; Yang, P.; Tilley, T. D. A Dimeric Molecular Precursor $[(tBuO)_2Ti\{\mu\text{-}O_2Si[OSi(OtBu)_3]_2\}]_2$ to Ti(IV)/SiO_2catalysts for Selective Cyclohexene Epoxidation. *J. Mol. Catal. A Chem.* **2005**, *238*, 1–12.

(39) Bordiga, S.; Damin, A.; Bonino, F.; Ricchiardi, G.; Lamberti, C.; Zecchina, A. The Structure of the Peroxo Species in the TS-1 Catalyst as Investigated by Resonant Raman Spectroscopy. *Angew. Chem. Int. Ed.* **2002**, *41*, 4734–4737.

(40) Ricchiardi, G.; Damin, A.; Bordiga, S.; Lamberti, C.; Spano, G.; Rivetti, F.; Zecchina, A.; Spanò, G.; Rivetti, F.; Zecchina, A. Vibrational Structure of Titanium Silicate Catalysts. A Spectroscopic and Theoretical Study. *J. Am. Chem. Soc.* **2001**, *123*, 11409–11419.

(41) Bordiga, S.; Damin, A.; Bonino, F.; Zecchina, A.; Spanò, G.; Rivetti, F.; Bolis, V.; Prestipino, C.; Lamberti, C. Effect of Interaction with H2O and NH3 on the Vibrational, Electronic, and Energetic Peculiarities of Ti(IV) Centers TS-1 Catalysts: A Spectroscopic and Computational Study. *J. Phys. Chem. B* **2002**, *106*, 9892–9905.

(42) Bordiga, S.; Damin, A.; Bonino, F.; Ricchiardi, G.; Zecchina, A.; Tagliapietra, R.; Lamberti, C. Resonance Raman Effects in TS-1: The Structure of Ti(IV) Species and Reactivity towards H_2O, NH_3 and H_2O_2: An in Situ Study. *Phys. Chem. Chem. Phys.* **2003**,

5, 4390–4393.

(43) Guo, Q.; Feng, Z.; Li, G.; Fan, F.; Li, C. Finding the "Missing Components" during the Synthesis of TS-1 Zeolite by UV Resonance Raman Spectroscopy. *J. Phys. Chem. C* **2013**, *117*, 2844–2848.

(44) Li, C.; Xiong, G.; Liu, J.; Ying, P.; Xin, Q.; Feng, Z. Identifying Framework Titanium in TS-1 Zeolite by UV Resonance Raman Spectroscopy. *J. Phys. Chem. B* **2001**, *105*, 2993–2997.

(45) Millini, R.; Massara, E. P.; Perego, G.; Bellussi, G.; Previde Massara, E.; Perego, G.; Bellussi, G. Framework Composition of Titanium Silicalite-1. *J. Catal.* **1992**, *137*, 497–503.

(46) Gleeson, D.; Sankar, G.; Catlow, C. R. A.; Thomas, J. .; Spano, G.; Bordiga, S.; Zecchina, A.; Lamberti, C. The Architecture of Catalytically Active Centers in Titanosilicate (TS-1) and Related Selective-Oxidation Catalysts. *Phys. Chem. Chem. Phys.* **2000**, *2*, 1–6.

(47) Lin, W.; Frei, H. Photochemical and FT-IR Probing of the Active Site of Hydrogen Peroxide in Ti Silicalite Sieve. *J. Am. Chem. Soc.* **2002**, *124*, 9292–9298.

(48) Tozzola, G.; Mantegazza, M. A.; Ranghino, G.; Petrini, G.; Bordiga, S.; Ricchiardi, G.; Lamberti, C.; Zulian, R.; Zecchina, A. On the Structure of the Active Site of Ti-Silicalite in Reactions with Hydrogen Peroxide: A Vibrational and Computational Study. *J. Catal.* **1998**, *179*, 64–71.

(49) Gale, J. D. A Periodic Density Functional Study of the Location of Titanium within TS-1. *Solid State Sci.* **2006**, *8*, 234–240.

(50) Gamba, A.; Tabacchi, G.; Fois, E. TS-1 from First Principles. *J. Phys. Chem. A* **2009**, *113*, 15006–15015.

(51) Montejo-Valencia, B. D.; Salcedo-Pérez, J. L.; Curet-Arana, M. C. DFT Study of Closed and Open Sites of BEA, FAU, MFI, and BEC Zeolites Substituted with Tin and Titanium. *J. Phys. Chem. C* **2016**, *120*, 2176–2186.

(52) Dong, J.; Zhu, H.; Xiang, Y.; Wang, Y.; An, P.; Gong, Y.; Liang, Y.; Qiu, L.; Zheng, A.; Peng, X.; et al. Toward a Unified Identification of Ti Location in the MFI Framework of High-Ti-Loaded TS-1: Combined EXAFS, XANES, and DFT Study. *J. Phys. Chem. C* **2016**, *120*, 20114–20124.

(53) To, J.; Sokol, A. A.; French, S. A.; Catlow, C. R. A. Hybrid QM/MM Investigations into the Structure and Properties of Oxygen-Donating Species in TS-1. *J. Phys. Chem. C* **2008**, *112*, 7173–7185.

(54) Signorile, M.; Damin, A.; Bonino, F.; Crocellà, V.; Ricchiardi, G.; Lamberti, C.; Bordiga, S. Computational Assessment of Relative Sites Stabilities and Site-Specific Adsorptive Properties of Titanium Silicalite-1. *J. Phys. Chem. C* **2018**, *122*, 1612–1621.

(55) Atoguchi, T.; Yao, S. Ti Atom in MFI Zeolite Framework: A Large Cluster Model Study by ONIOM Method. *J. Mol. Catal. A Chem.* **2003**, *191*, 281–288.

(56) Panyaburapa, W.; Nanok, T.; Limtrakul, J. Epoxidation Reaction of Unsaturated Hydrocarbons with H_2O_2 over Defect TS-1 Investigated by ONIOM Method: Formation of Active Sites and Reaction Mechanisms. *J. Phys. Chem. C* **2007**, *111*, 3433–3441.

(57) Nie, X.; Ji, X.; Chen, Y.; Guo, X.; Song, C. Mechanistic Investigation of Propylene Epoxidation with H_2O_2 over TS-1: Active Site Formation, Intermediate Identification, and Oxygen Transfer Pathway. *Mol. Catal.* **2017**, *441*, 150–167.

(58) Su, J.; Xiong, G.; Zhou, J.; Liu, W.; Zhou, D.; Wang, G.; Wang, X.; Guo, H. Amorphous Ti Species in Titanium Silicalite-1: Structural Features, Chemical Properties, and

Inactivation with Sulfosalt. *J. Catal.* **2012**, *288*, 1–7.

(59) Zuo, Y.; Liu, M.; Zhang, T.; Hong, L.; Guo, X.; Song, C.; Chen, Y.; Zhu, P.; Jaye, C.; Fischer, D. Role of Pentahedrally Coordinated Titanium in Titanium Silicalite-1 in Propene Epoxidation. *RSC Adv.* **2015**, *5*, 17897–17904.

(60) Song, W.; Xiong, G.; Long, H.; Jin, F.; Liu, L.; Wang, X. Effect of Treatment with Different Bases on the Catalytic Properties of TS-1/SiO_2 Extrudates in Propylene Epoxidation. *Microporous Mesoporous Mater.* **2015**, *212*, 48–55.

(61) Yang, G.; Lan, X.; Zhuang, J.; Ma, D.; Zhou, L.; Liu, X.; Han, X.; Bao, X. Acidity and Defect Sites in Titanium Silicalite Catalyst. *Appl. Catal. A Gen.* **2008**, *337*, 58–65.

(62) Blasco, T.; Camblor, M. A.; Corma, A.; Perez-Pariente, J. The State of Ti in Titanoaluminosilicates Isomorphous with Zeolite Beta. *J. Am. Chem. Soc.* **1993**, *115*, 11806–11813.

(63) Fan, W.; Duan, R. G.; Yokoi, T.; Wu, P.; Kubota, Y.; Tatsumi, T. Synthesis, Crystallization Mechanism, and Catalytic Properties of Titanium-Rich TS-1 Free of Extraframework Titanium Species. *J. Am. Chem. Soc.* **2008**, *130*, 10150–10164.

(64) Wells, D. H.; Joshi, A. M.; Delgass, W. N.; Thomson, K. T. A Quantum Chemical Study of Comparison of Various Propylene Epoxidation Mechanisms Using H_2O_2 and TS-1 Catalyst. *J. Phys. Chem. B* **2006**, *110*, 14627–14639.

(65) Limtrakul, J.; Inntam, C.; Truong, T. N. Density Functional Theory Study of the Ethylene Epoxidation over Ti-Substituted Silicalite (TS-1). *J. Mol. Catal. A Chem.* **2004**, *207*, 139–148.

(66) Catlow, C. R. A.; French, S. A.; Sokol, A. A.; Thomas, J. M. Computational Approaches to the Determination of Active Site Structures and Reaction Mechanisms in

Heterogeneous Catalysts. *Philos. Trans. R. Soc. A Math. Phys. Eng. Sci.* **2005**, *363*, 913–936.

(67) Guo, Q.; Sun, K.; Feng, Z.; Li, G.; Guo, M.; Fan, F.; Li, C. A Thorough Investigation of the Active Titanium Species in TS-1 Zeolite by in Situ UV Resonance Raman Spectroscopy. *Chem. Eur. J.* **2012**, *18*, 13854–13860.

(68) Artioli, G.; Lamberti, C.; Marra, G. L. Neutron Powder Diffraction Study of Orthorhombic and Monoclinic Defective Silicalite. *Acta Crystallogr. Sect. B Struct. Sci.* **2000**, *56*, 2–10.

(69) Bordiga, S.; Roggero, I.; Ugliengo, P.; Zecchina, A.; Bolis, V.; Artioli, G.; Buzzoni, R.; Marra, G.; Rivetti, F.; Spanò, G.; et al. Characterisation of Defective Silicalites. *J. Chem. Soc., Dalton Trans.* **2000**, *21*, 3921–3929.

(70) Bordiga, S.; Ugliengo, P.; Damin, A.; Lamberti, C.; Spoto, G.; Zecchina, A.; Spano, G.; Buzzoni, R.; Dalloro, L.; Rivetti, F. Hydroxyls Nests in Defective Silicalites and Strained Structures Derived upon Dehydroxylation: Vibrational Properties and Theoretical Modelling. *Top. Catal.* **2001**, *15*, 43–52.

(71) Wu, L.; Zhao, S.; Lin, L.; Fang, X.; Liu, Y.; He, M. In-Depth Understanding of Acid Catalysis of Solvolysis of Propene Oxide over Titanosilicates and titanosilicate/H_2O_2 Systems. *J. Catal.* **2016**, *337*, 248–259.

(72) Mirajkar, S. P.; Thangaraj, A.; Shiralkar, V. P. Sorption Properties of Titanium Silicate Molecular Sieves. *J. Phys. Chem.* **1992**, *96*, 3073–3079.

(73) D'amico, F.; Saito, M.; Bencivenga, F.; Marsi, M.; Gessini, A.; Camisasca, G.; Principi, E.; Cucini, R.; Di Fonzo, S.; Battistoni, A.; et al. UV Resonant Raman Scattering Facility at Elettra. *Nucl. Instruments Methods Phys. Res. Sect. A Accel. Spectrometers, Detect.*

Assoc. Equip. **2013**, *703*, 33–37.

(74) Cicco, A. Di; Aquilanti, G.; Minicucci, M.; Principi, E.; Novello, N.; Cognigni, A.; Olivi, L. Novel XAFS Capabilities at ELETTRA Synchrotron Light Source. In *Journal of Physics: Conference Series*; 2009; Vol. 190.

(75) Lamberti, C.; Bordiga, S.; Bonino, F.; Prestipino, C.; Berlier, G.; Capello, L.; D'Acapito, F.; Llabrés i Xamena, F. X.; Zecchina, A. Determination of the Oxidation and Coordination State of Copper on Different Cu-Based Catalysts by XANES Spectroscopy in Situ or in Operando Conditions. *Phys. Chem. Chem. Phys.* **2003**, *5*, 4502–4509.

(76) Lamberti, C.; Prestipino, C.; Bordiga, S.; Berlier, G.; Spoto, G.; Zecchina, A.; Laloni, A.; La Manna, F.; D'Anca, F.; Felici, R.; et al. Description of a Flexible Cell for in Situ X-Ray and Far-IR Characterization of the Surface of Powdered Materials. In *Nuclear Instruments and Methods in Physics Research, Section B: Beam Interactions with Materials and Atoms*; 2003; Vol. 200, pp 196–201.

(77) Boccuti, M. R.; Rao, K. M.; Zecchina, A.; Leofanti, G.; Petrini, G. Spectroscopic Characterization of Silicalite and Titanium-Silicalite. *Stud. Surf. Sci. Catal.* **1989**, *48C*, 133–144.

(78) Geobaldo, F.; Bordiga, S.; Zecchina, A.; Giamello, E.; Leofanti, G.; Petrini, G. DRS UV-Vis and EPR Spectroscopy of Hydroperoxo and Superoxo Complexes in Titanium Silicalite. *Catal. Letters* **1992**, *16*, 109–115.

(79) Borello, E.; Lamberti, C.; Bordiga, S.; Zecchina, A.; Areán, C. O. Quantum-Size Effects in the Titanosilicate Molecular Sieve. *Appl. Phys. Lett.* **1997**, *71*, 2319.

(80) Lamberti, C. Electron–hole Reduced Effective Mass in Monoatomic …–O–Ti–O–Ti–O–… Quantum Wires Embedded in the Siliceous Crystalline Matrix of ETS-10. *Microporous*

Mesoporous Mater. **1999**, *30*, 155–163.

(81) Amtout, A.; Leonelli, R. Optical Properties of Rutile near Its Fundamental Band Gap. *Phys*. *Rev*. *B* **1995**, *51*, 6842–6851.

(82) Tang, H.; Lévy, F.; Berger, H.; Schmid, P. E. Urbach Tail of Anatase TiO_2. *Phys*. *Rev*. *B* **1995**, *52*, 7771–7774.

(83) Mattsson, A.; Österlund, L. Adsorption and Photoinduced Decomposition of Acetone and Acetic Acid on Anatase, Brookite, and Rutile TiO_2 Nanoparticles. *J*. *Phys*. *Chem*. *C* **2010**, *114*, 14121–14132.

(84) Fan, F.; Feng, Z.; Li, C. UV Raman Spectroscopic Studies on Active Sites and Synthesis Mechanisms of Transition Metal-Containing Microporous and Mesoporous Materials. *Acc*. *Chem*. *Res*. **2010**, *43*, 378–387.

(85) Li, C.; Xiong, G.; Xin, Q.; Liu, J. K.; Ying, P. L.; Feng, Z. C.; Li, J.; Yang, W. Bin; Wang, Y. Z.; Wang, G. R.; et al. UV Resonance Raman Spectroscopic Identification of Titanium Atoms in the Framework of TS-1 Zeolite. *Angew*. *Chem*. *Int*. *Ed*. **1999**, *38*, 2220–2222.

(86) Scarano, D.; Zecchina, A.; Bordiga, S.; Geobaldo, F.; Spoto, G.; Petrini, G.; Leofanti, G.; Padovan, M.; Tozzola, G. Fourier-Transform Infrared and Raman Spectra of Pure and Al-, B-, Ti- and Fe-Substituted Silicalites: Stretching-Mode Region. *J*. *Chem*. *Soc*. *Faraday Trans*. **1993**, *89*, 4123–4130.

(87) Knops-Gerrits, P.-P.; De Vos, D. E.; Feijen, E. J. P.; Jacobs, P. A. Raman Spectroscopy on Zeolites. *Microporous Mater*. **1997**, *8*, 3–17.

(88) Bordiga, S.; Coluccia, S.; Lamberti, C.; Marchese, L.; Zecchina, A.; Boscherini, F.; Buffa, F.; Genoni, F.; Leofanti, G.; Petrini, G.; et al. XAFS Study of Ti-Silicalite: Structure of

Framework Ti(IV) in the Presence and Absence of Reactive Molecules (H_2O, NH_3) and Comparison with Ultraviolet-Visible and IR Results. *J. Phys. Chem.* **1994**, *98*, 4125–4132.

(89) Davis, R. J.; Liu, Z.; Tabora, J. E.; Wieland, W. S. X-Ray Absorption Spectroscopy of Ti-Containing Molecular Sieves ETS-10, Aluminum-Free Ti-B, and TS-1. *Catal. Letters* **1995**, *34*, 101–113.

(90) Wu, Z.; Ouvrard, G.; Gressier, P. Ti and O K Edges for Titanium Oxides by Multiple Scattering Calculations: Comparison to XAS and EELS Spectra. *Phys. Rev. B* **1997**, *55*, 10382–10391.

(91) Cabaret, D.; Joly, Y.; Renevier, H.; Natoli, C. R. Pre-Edge Structure Analysis of Ti K-Edge Polarized X-Ray Absorption Spectra in TiO_2 by Full-Potential XANES Calculations. *J. Synchrotron Radiat.* **1999**, *6*, 258–260.

(92) Boccuzzi, F.; Coluccia, S.; Ghiotti, G.; Morterra, C.; Zecchina, A. Infrared Study of Surface Modes on Silica. *J. Phys. Chem.* **1978**, *82*, 1298–1303.

(93) Lamberti, C.; Bordiga, S.; Zecchina, A.; Artioli, G.; Marra, G.; Spanò, G. Ti Location in the MFI Framework of Ti-Silicalite-1: A Neutron Powder Diffraction Study. *J. Am. Chem. Soc.* **2001**, *123*, 2204–2212.

(94) Bonino, F.; Damin, A.; Bordiga, S.; Lamberti, C.; Zecchina, A. Interaction of CD_3CN and Pyridine with the Ti(IV) Centers of TS-1 Catalysts: A Spectroscopic and Computational Study. *Langmuir* **2003**, *19*, 2155–2161.

(95) Ohsaka, T.; Izumi, F.; Fujiki, Y. Raman Spectrum of Anatase, TiO_2. *J. Raman Spectrosc.* **1978**, *7*, 321–324.

(96) Bolis, V.; Busco, C.; Bordiga, S.; Ugliengo, P.; Lamberti, C.; Zecchina, A. Calorimetric and IR Spectroscopic Study of the Interaction of NH3 with Variously Prepared Defective

Silicalites: Comparison with Ab Initio Computational Data. *Appl. Surf. Sci.* **2002**, *196*, 56–70.

(97) Zecchina, A.; Bordiga, S.; Spoto, G.; Marchese, L.; Petrini, G.; Leofanti, G.; Padovan, M. Silicalite Characterization. 2. IR Spectroscopy of the Interaction of Carbon Monoxide with Internal and External Hydroxyl Groups. *J. Phys. Chem.* **1992**, *96*, 4991–4997.

(98) Armaroli, T.; Milella, F.; Notari, B.; Willey, R. J.; Busca, G. A Spectroscopic Study of Amorphous and Crystalline Ti-Containing Silicas and Their Surface Acidity. *Top. Catal.* **2001**, *15*, 63–71.

(99) Zecchina, A.; Spoto, G.; Bordiga, S.; Padovan, M.; Leofanti, G.; Petrini, G. IR Spectra of Co Adsorbed at Low Temperature (77 K) on Titaniumsilicalite, H-ZSM5 and Silicalite. *Stud. Surf. Sci. Catal.* **1991**, *65C*, 671–680.

(100) Holm, M. S.; Svelle, S.; Joensen, F.; Beato, P.; Christensen, C. H.; Bordiga, S.; Bjørgen, M. Assessing the Acid Properties of Desilicated ZSM-5 by FTIR Using CO and 2,4,6-Trimethylpyridine (Collidine) as Molecular Probes. *Appl. Catal. A Gen.* **2009**, *356*, 23–30.

(101) Bordiga, S.; Lamberti, C.; Bonino, F.; Travert, A.; Thibault-Starzyk, F. Probing Zeolites by Vibrational Spectroscopies. *Chem. Soc. Rev.* **2015**, *44*, 7262–7341.

(102) Xin, H.; Zhao, J.; Xu, S.; Li, J.; Zhang, W.; Guo, X.; Hensen, E. J. M.; Yang, Q.; Li, C. Enhanced Catalytic Oxidation by Hierarchically Structured TS-1 Zeolite. *J. Phys. Chem. C* **2010**, *114*, 6553–6559.

(103) Russo, V.; Tesser, R.; Santacesaria, E.; Di Serio, M. Kinetics of Propene Oxide Production via Hydrogen Peroxide with TS-1. *Ind. Eng. Chem. Res.* **2014**, *53*, 6274–6287.

TOC Graphic